Dong et al., http://www.jcb.org/cgi/content/full/jcb.201503067/DC1

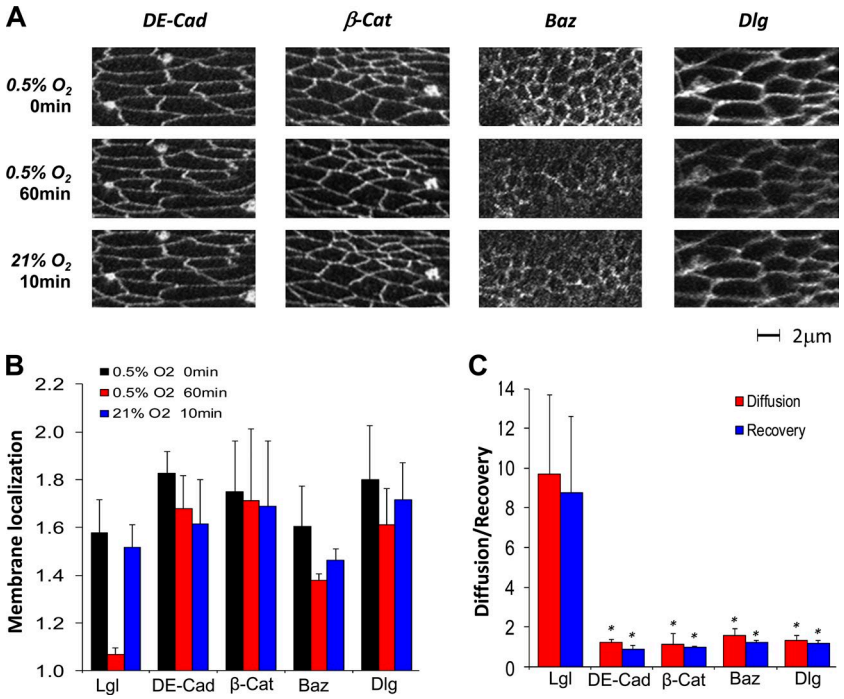


Figure S1. **Hypoxia does not disrupt cell polarity.** (A) Subcellular localization of DE-Cad::GFP, β-Cat::GFP, Baz::GFP, and Dlg::GFP in embryonic epithelia under hypoxia and post-hypoxia reoxygenation. All embryos are at approximately late stage 15, except for *baz::GFP* embryo, which is at early embryonic stage 11. (B and C) Quantification of membrane localization (C) and the indices of diffusion and recovery (D) of Lgl::GFP, DE-Cad::GFP, β-Cat::GFP, Baz::GFP, and Dlg::GFP during hypoxia treatment. See Materials and methods for quantification details. *, $P < 0.05$. Error bars represent means ± SEM.

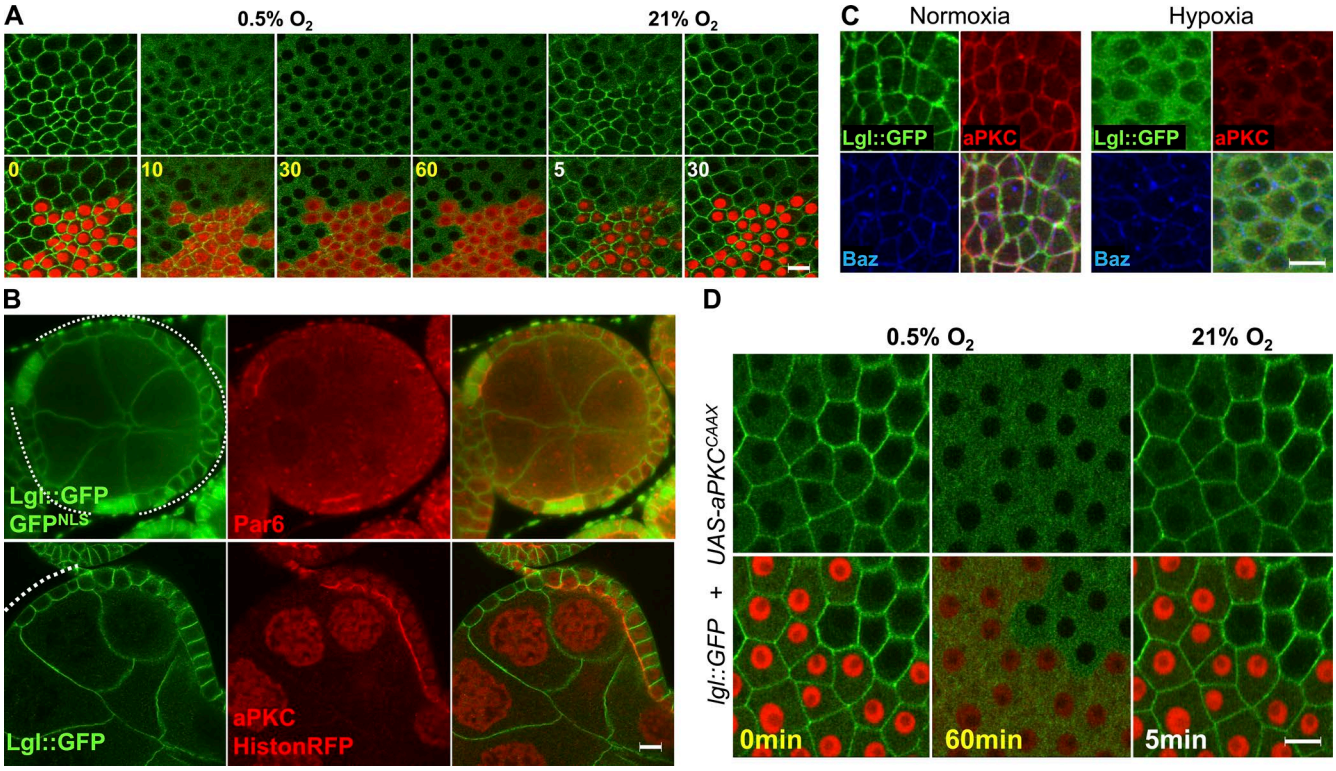


Figure S2. **Inhibition of Lgl PM targeting is modulated by HIF activity but is independent of aPKC/Par-6 complex.** (A) Lgl::GFP showed delayed diffusion in follicular epithelial cells overexpressing Sima (marked by RFP). (B) Ovaries bearing *par-6* or *aPKC* mutant clones from *lgl::GFP* females were double stained with anti-GFP and anti–Par-6 or anti-aPKC antibodies. Loss of nuclear GFP or RFP marks the *par-6* and *aPKC* clones, respectively. Par-6 and aPKC proteins have strong expression in wild-type cells but become undetectable in mutant cells (highlighted by dash lines). (C) Loss of PM targeting of aPKC and Lgl::GFP but not Baz in hypoxia-treated embryos. (D) Lgl::GFP show partial loss of PM targeting in follicular cells expressing membrane-bound $aPKC^{CAAX}$ (marked by nuclear RFP) but normal response to hypoxia and reoxygenation. Bars, 5 µm.

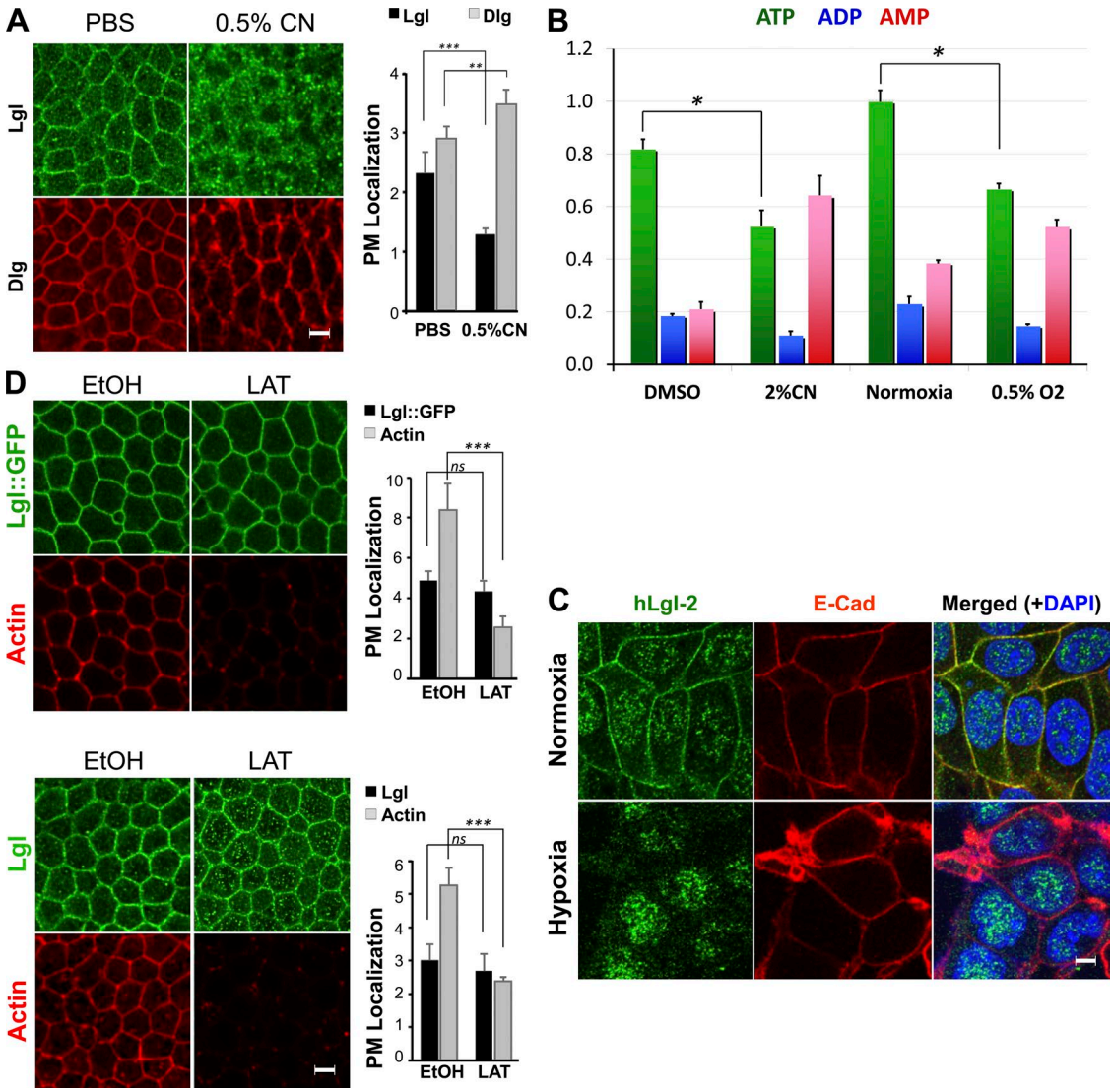


Figure S3. **Hypoxia inhibits Lgl PM targeting through reducing intracellular ATP levels.** (A) Loss of PM targeting in endogenous Lgl in sodium cyanide (CN)-treated embryos. (B) Intracellular ATP, ADP, and AMP levels in hypoxia- or cyanide-treated embryos as well as controls. Concentrations of ATP, ADP, and AMP were measured against the ATP levels in normoxia-treated embryos. Hypoxia and cyanide treatments induced a clear reduction of ATP levels and commensurate increase of AMP levels. (C) Loss of PM localization of hLgl-2 (green) but not E-cadherin (E-Cad; red) in hypoxia-treated MCF7 cells. hLgl-2 antibody also shows nuclear signal, which is likely caused by reactions to nonspecific antigens. (D) Lgl::GFP and endogenous Lgl remain PM targeted in latrunculin-treated embryos. After latrunculin treatment, both *lgl::GFP* and wild-type embryos were fixed and hand devitellinized. Lgl::GFP embryos were imaged with TRITC-phalloidin staining only, whereas wild-type embryos were immunostained with anti-Lgl antibody (green) and TRITC-phalloidin ($n$ = 6 for each sample). *, $P < 0.05$; **, $P < 0.01$; ***, $P < 0.001$. *ns*, not significant. Bars, 5 µm. Error bars represent means ± SEM.

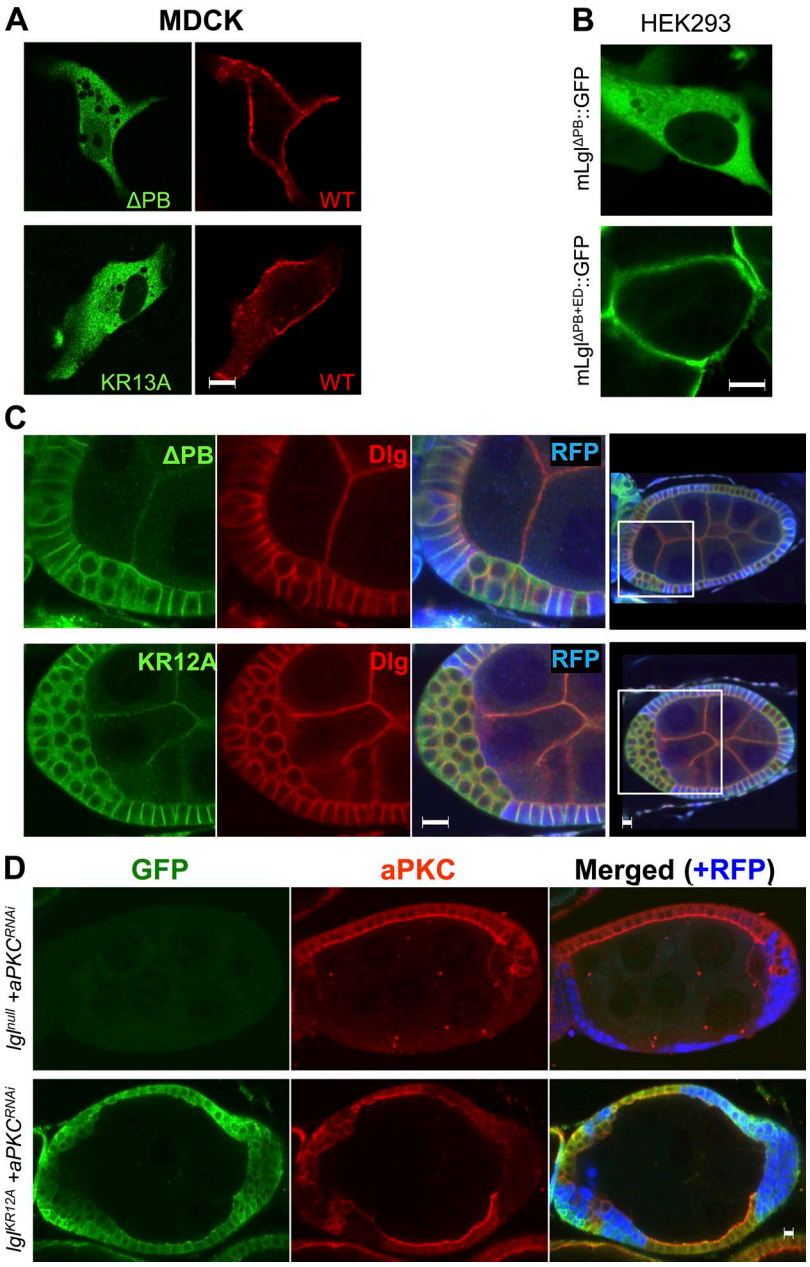


Figure S4. **PB domain mediates the PM targeting of Lgl in both mammalian and *Drosophila* cells.** (A) MDCK cells were expressing both mLgl::RFP and mLgl$^{\Delta PB}$::GFP (ΔPB) or mLgl$^{KR13A}$::GFP (KR13A). In the same cell, while mLgl::RFP localizes PM, mLgl$^{\Delta PB}$::GFP or mLgl$^{KR13A}$::GFP is cytosolic. (B) Replacing the PB domain in mLgl with MARCKS PB ED domain (i.e., mLgl$^{\Delta PB+ED}$::GFP) rescues the loss of PM targeting of mLgl$^{\Delta PB}$::GFP in HEK293 cells. Sequence of MARCKS ED domain: KKKKKRFSFKKSFKLSGFSFKKNKK. (C) Cortical localization of Dlg (red) is no longer restricted to the basolateral domain in *lgl$^{\Delta PB}$::GFP* or *lgl$^{KR12A}$::GFP* mutant follicular cells (labeled by the loss of GFP; blue). White boxes in the left of most panels highlight the area enlarged in right panels. (D) Knocking down aPKC by RNAi in follicular cell clones of *lgl$^{null}$* or *lgl$^{KR12A}$::GFP* does not rescue their overproliferation and multilayered phenotypes. *lgl$^{null}$* or *lgl$^{KR12A}$::GFP* mutant clones were generated by MARCM technique to simultaneously express RFP and aPKC-RNAi. The efficiency of aPKC-RNAi was confirmed by the loss of aPKC staining RFP-labeled clones.

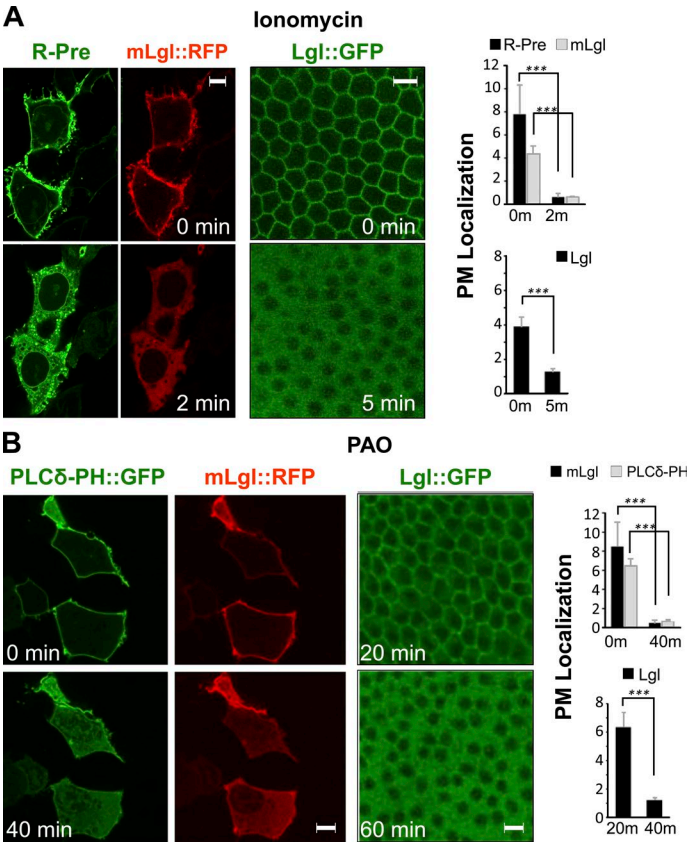


Figure S5. **PM phospholipids are required for targeting Lgl.** (A and B) Both ionomycin and PAO treatments induced diffusion of mLgl::RFP from PM in HEK293 cells ($n$ = 4), as well as Lgl::GFP diffusion in *Drosophila* follicular epithelial cells ($n$ = 4). Different ionomycin-treated samples were imaged at 0 min, and R-pre::GFP is a probe that specifically binds to charged PM (Yeung et al., 2006). ***, $P < 0.001$. Bars, 5 µm. Error bars represent means ± SEM.

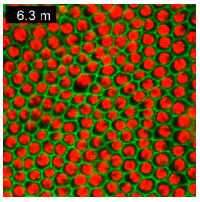


Video 1. **Time-lapse recording of Lgl::GFP and His2Av::RFP in follicular cells under hypoxia and reoxygenation.** Dissected ovaries from a 3-d-old *lgl::GFP his2Av::RFP* female were imaged live in a micro chamber. Hypoxic (0.5% $O_2$) gas was introduced into the chamber at 2.2 min of recording, and the steady gas flow persisted until 39.3 min. Hypoxic gas was then replaced by normal airflow for reoxygenation. The sudden shifts of focus of video frame at 2.2 and 39.3 min are caused by the chamber pressure fluctuations as a result of gas source switching. Images were analyzed by time-lapse confocal microscopy using a laser-scanning confocal microscope (LSM 510; Carl Zeiss). Frames were taken every 19 s for 48.8 min under hypoxia.

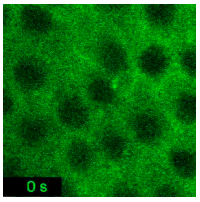


Video 2. **PM relocalization of Lgl::GFP during post-hypoxia reoxygenation.** Dissected ovary from a 3-d-old *lgl::GFP* female was exposed to hypoxia for 45 min. The video starts at the beginning of reoxygenation during which time oxygen apparently diffuses from the top right corner of the follicular tissue to the bottom left corner. Images were analyzed by time-lapse confocal microscopy using a laser-scanning confocal microscope (LSM 510; Carl Zeiss). Frames were taken every 2 s for 6 min.

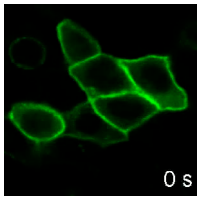


Video 3. **PM targeting of mLgl::GFP in MDCK cells under hypoxia and reoxygenation.** MDCK cells cultured for 3 d in MEMα medium on 12-mm diameter filters (pore size, 0.4 µm) were mounted and imaged in custom micro-imaging chambers under a steady temperature of 37°C. Flow of hypoxic gas mixture of 1% $O_2$/5% $CO_2$/94% $N_2$ into the imaging chamber starts at 0 s and persists until 2,340 s. Gas flow was then switched to normal air until the end of recording. Images were analyzed by time-lapse confocal microscopy using a laser-scanning confocal microscope (LSM 510; Carl Zeiss). Frames were taken every minute for 39 min under hypoxia and every 15 s for 19 min after hypoxia.

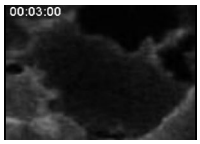


Video 4. **Recovery of PM targeting of mLgl::GFP in hypoxia-treated HEK293 cells.** HEK293 cells were treated in a hypoxia chamber for 72 h under 0.5% $O_2$ and then were allowed to recover under normoxia. Images were analyzed by time-lapse confocal microscopy using a laser-scanning confocal microscope (A1; Nikon). Note that the time interval is not constant, and frames were taken at the time points indicated in the video.

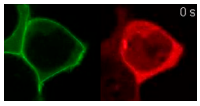


Video 5. **Inhibition of mLgl::GFP PM targeting by rapamycin-induced PM recruitment of PJ::RFP in HEK293 cells.** Subcellular relocalization of mLgl::GFP and FKBP12-PJ::RFP in HEK293 cells in response to rapamycin treatment. HEK293 cells were triple transfected with mLgl::GFP, FKBP12-PJ::RFP, and PM-FRB-CFP. 24 h after transfection, 5 µM rapamycin was added to the cells. Images were analyzed by time-lapse confocal microscopy using a laser-scanning confocal microscope (A1; Nikon). Frames were taken every 20 s for 440 s.

**An ImageJ_Macro-1.txt file, provided online, is an ImageJ macro used to measure cortical Lgl::GFP localization.**

## References

Yeung, T., M. Terebiznik, L. Yu, J. Silvius, W.M. Abidi, M. Philips, T. Levine, A. Kapus, and S. Grinstein. 2006. Receptor activation alters inner surface potential during phagocytosis. *Science.* 313:347–351. http://dx.doi.org/10.1126/science.1129551